NANOSYSTEMS:
PHYSICS, CHEMISTRY, MATHEMATICS

Original article

Martinson K.D., et al. *Nanosystems: Phys. Chem. Math.*, 2024, **15** (2), 233–239.
http://nanojournal.ifmo.ru
DOI 10.17586/2220-8054-2024-15-2-233-239

Structural, magnetic and electrochemical studies on $Zn_xMg_{1-x}Fe_2O_4$ nanoparticles prepared via solution combustion method

Kirill D. Martinson[1,a], Alexander A. Murashkin[2,b], Artem A. Lobinsky[1,c], Danil D. Maltsev[1,d], Kezhen Qi[3,e], Jiaguo Yu[4,f], Oksana V. Almjasheva[2,g], Vadim I. Popkov[1,h]

[1]Ioffe Institute, Saint Petersburg, Russia

[2]Saint Petersburg Electrotechnical University "LETI", Saint Petersburg, Russia

[3] College of Pharmacy, Dali University, Dali, China

[4] China University of Geosciences, Wuhan, China

[a]martinsonkirill@mail.ru, [b]murashkin1999@list.ru, [c]lobinski.a@mail.ru, [d]dm.work.ac@gmail.com, [e]qkzh2003@aliyun.com, [f]yujiaguo93@cug.edu.cn, [g]almjasheva@mail.ru, [h]vip-07@yandex.ru

Corresponding author: K. D. Martinson, martinsonkirill@mail.ru

PACS 61.46Df, 75.50.Gg, 75.75.Fk

ABSTRACT Zinc-manganese ferrite nanoparticles, denoted as $Zn_xMg_{1-x}Fe_2O_4$ where x ranges from 0 to 1, were synthesized via solution combustion employing glycine as the organic fuel at a stoichiometric redox ratio. The resultant compositions underwent comprehensive characterization utilizing scanning electron microscopy, energy-dispersive spectroscopy, and powder X-ray diffractometry. Magnetic and electrochemical properties were meticulously examined using a vibrating magnetometer and cyclic voltmeter, respectively. Analysis revealed an average particle size ranging from 24.9 to 30.8 nm across all synthesized samples, with degrees of crystallinity reaching 93–96%. Notably, variations in the magnetic behavior were observed depending on the magnesium content within the samples. The highest magnetic parameters were recorded for $Zn_{0.4}Mg_{0.6}Fe_2O_4$ (M_s = 27.78 emu/g, M_r = 3.77 emu/g, and H_c = 21.4 Oe). Furthermore, the electrochemical capacity of the synthesized powders exhibited dependency on the incorporation of magnesium cations into the crystal lattice. These findings underscore the significance of magnesium content in modulating the magnetic and electrochemical properties of $Zn_xMg_{1-x}Fe_2O_4$ nanoparticles synthesized via solution combustion.

KEYWORDS zinc-manganese ferrite, nanoparticles, magnetic properties, electrochemical properties.

ACKNOWLEDGEMENTS The reported study was funded by Russian Science Foundation (grant no. 21-73-10070).

FOR CITATION Martinson K.D., Murashkin A.A., Lobinsky A.A., Maltsev D.D., Qi K., Yu J., Almjasheva O.V., Popkov V.I. Structural, magnetic and electrochemical studies on $Zn_xMg_{1-x}Fe_2O_4$ nanoparticles prepared via solution combustion method. *Nanosystems: Phys. Chem. Math.*, 2024, **15** (2), 233–239.

1. Introduction

Spinel ferrites represent a crucial category of industrial materials renowned for their diverse functional properties, rendering them applicable across a broad spectrum [1]. This class encompasses compounds with the general chemical formula AFe_2O_4, wherein A denotes a divalent metal cation (such as Co, Ni, Zn, Mn, Mg, or Li). Notably, ferrites find significant utility in the realm of radio-electronic devices, with multicomponent lithium and nickel ferrites serving as pivotal components in the production of microwave ceramic products [2]. The prevalence of spinel ferrites in this domain stems from their distinctive magnetic and electromagnetic attributes, which exhibit variability across a wide range, often facilitated by the incorporation of transition metal cations [3]. Moreover, the incorporation of various metal cations within the crystal lattice of spinels has spurred their application in the fabrication of phase shifters, transformer cores, ferrite filters, and etc. [4].

Among spinel ferrites, multicomponent zinc ferrites assume particular significance. Pure zinc ferrite is classified as a normal spinel, characterized by the presence of 8 divalent Zn^{2+} cations at tetrahedral positions and 16 trivalent Fe^{3+} cations at octahedral positions [5]. Conversely, magnesium ferrite belongs to the inverted spinel category, with 8 divalent Mg^{2+} cations occupying 8 of the 16 available octahedral positions, and 16 trivalent Fe^{3+} cations distributed between 8 tetrahedral and 8 octahedral positions [6]. The replacement of zinc cations with magnesium counterparts at octahedral positions induces structural alterations, thereby dictating the magnetic and electromagnetic behavior of multicomponent zinc-magnesium ferrites [7]. Industrially, multicomponent magnesium and zinc ferrites find widespread application in microwave electronics, as well as in the manufacture of various sensors and transmitters [8]. Notably, the advent of

nanomaterials has ushered in new avenues for the utilization of spinel ferrites, including catalytic and photocatalytic applications [9], wastewater treatment [10], antibacterial materials [11], and MRI contrast agents [12]. However, the synthesis of ferrite nanopowders poses challenges, particularly with conventional solid-phase synthesis methods, owing to difficulties in obtaining pure single-phase samples with particles in the range of 30–40 nm [12]. Consequently, there is a pressing need to explore and develop methodologies for producing ferrite nanoparticles.

Presently, numerous methods exist for synthesizing nanopowders of multicomponent zinc-magnesium ferrites [13], including hydrothermal synthesis [14], sonochemical synthesis [15], co-precipitation method, various types of solution combustion methods [16], synthesis in activator mills [17] and sol-gel technology [18]. Notably, the solution combustion method has garnered attention due to its simplicity, cost-effectiveness, and potential for industrial scalability, offering a pathway to volumetric yields akin to classical solid-phase techniques [19]. Recent efforts within this method have seen the synthesis of zinc-magnesium ferrites employing citric acid and microwave treatment [20,21]. Although standalone studies have synthesized pure zinc and magnesium ferrites via the solution combustion method using glycine as a fuel [22, 23], investigations into the physical and chemical processes governing the formation of the $Zn_xMg_{1-x}Fe_2O_4$ system (x = 0, 0.2, ..., 1.0), along with its magnetic and electrochemical properties, remain scarce.

Hence, the present study addresses the imperative to explore synthesis methodologies for multicomponent zinc-magnesium ferrites under solution combustion conditions, enabling the targeted fabrication of nanostructures. Glycine was chosen as the organic fuel due to its propensity for generating compositions with minimal amorphous content, particularly when used in stoichiometric proportions in the reaction solution. Herein, we report the synthesis of nanopowders with the composition $Zn_xMg_{1-x}Fe_2O_4$ (x = 0, 0.2, ..., 1.0) under glycine-nitrate combustion conditions, followed by comprehensive analysis employing modern physicochemical techniques.

2. Experimental

The following reagents were utilized for the synthesis: $Zn(NO_3)_2{\cdot}6H_2O$ (puriss., NevaReactiv), $Mg(NO_3)_2{\cdot}6H_2O$ (puriss., NevaReactiv), $Fe(NO_3)_3{\cdot}9H_2O$ (puriss., NevaReactiv), CH_2NH_2COOH (puriss., NevaReactiv), HNO_3 (puriss., NevaReactiv), and double distilled water. The original zinc, magnesium, and iron nitrates were dissolved in 50 ml of distilled water with constant mechanical stirring until complete dissolution was achieved. Subsequently, glycine was added to the initial reaction solution in a stoichiometric amount, calculated based on the reaction for the formation of the primary combustion products [16, 23]. A small quantity of 5M nitric acid was introduced to the solution to prevent the formation of complex products. The resulting reaction solution was then heated on a ceramic tile until reaching the autoignition point, resulting in the formation of gaseous and solid combustion products. The brown powder synthesized in this manner was collected from the reaction beaker, ground mechanically in a mortar, and subjected to thermal treatment in an air atmosphere at a temperature of 500°C for 1 hour to eliminate any unreacted organic reagents.

The elemental composition and morphological characteristics of the synthesized compositions were assessed using energy-dispersive spectroscopy and scanning electron microscopy via a Tescan Vega 3 SBH scanning electron microscope equipped with an Oxford INCA attachment. X-ray phase and structural analyses were conducted based on diffraction patterns obtained through powder X-ray diffractometry employing a Rigaku SmartLab 3 diffractometer. The primary shooting parameters selected were CuKα1 radiation (0.154056 nm) at 40 kV and 30 mA, covering a range from 20 to 80 degrees of 2θ, with increments of 0.01° and an exposition time of 3 seconds. The average crystallite size was determined utilizing the Scherrer formula, while the crystallite size distribution was assessed through the method of fundamental parameters. The proportion of crystalline and amorphous phases, as well as unit cell parameters, were calculated using the Rigaku SmartLab Studio II software package. Magnetic M-H hysteresis loops were obtained employing a Lake Shore 7410 vibrating magnetometer at room temperature (278 K) within a field range of up to 60,000 Oe utilizing a standard cell. Cyclic voltammetry (CVA) curves were recorded using a SmartStat PS-20 potentiostat equipped with an FRA module in an alkaline electrolyte of 1 M KOH, spanning from -1700 to 700 mV relative to the silver chloride electrode. For a sample deposition, a suspension with Nafion in isopropanol was prepared.

3. Results and Discussion

Fig. 1 illustrates the morphological characteristics of the synthesized samples, employing the $Zn_{0.6}Mg_{0.4}Fe_2O_4$ sample as a representative example. The data obtained reveal that the morphology of zinc-manganese ferrite nanopowders manifests as micron-scale agglomerates, ranging in size from 3 to 10 μm, composed of nanoparticles measuring approximately 20–30 nm. Notably, the appearance of these agglomerates demonstrates minimal variation across different compositions of Mg^{2+} cations within the crystal lattice, consistent with typical solid products resulting from solution combustion. Furthermore, Fig. 1f highlights the presence of amorphous bridges in certain regions, facilitating connections between individual particles, which exhibit a predominantly spherical morphology.

Based on the acquired microphotographs, a particle size distribution was generated using the ImageJ software package, as depicted in Fig. 2. Among the depicted distributions, the smallest average particle size is observed in the $Zn_{0.4}Mg_{0.6}Fe_2O_4$ sample, measuring 24.9 nm. Pure zinc and magnesium ferrites, along with $Zn_{0.2}Mg_{0.8}Fe_2O_4$ and $Zn_{0.8}Mg_{0.2}Fe_2O_4$, exhibit relatively consistent average particle sizes ranging from 28 to 31 nm. This observation suggests that the minimum size occurs within the range of magnesium cation content (x = 0.4 and 0.6), possibly attributed to

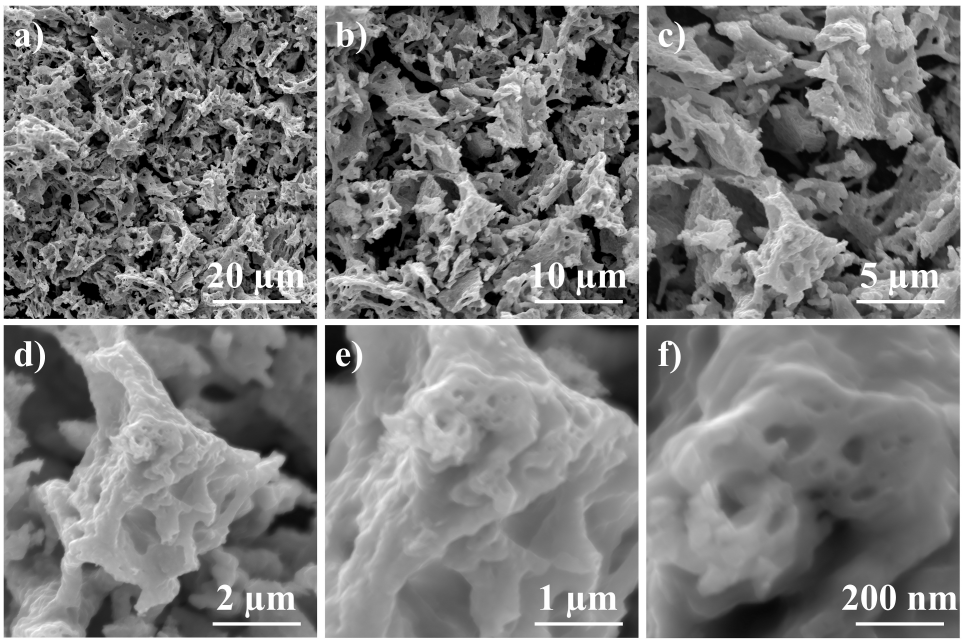

FIG. 1. SEM micrographs of $Zn_{0.6}Mg_{0.4}Fe_2O_4$ synthesized via solution combustion approach

the distribution patterns of zinc and manganese cations within the mixed spinel structure, as well as the composition of the initial reaction influencing the combustion temperature of the flame. Moreover, it is noteworthy to mention the distribution type; across all samples, there is an absence of a bimodal distribution pattern, with a distinct center of distribution evident. This indicates a high degree of uniformity in the size distribution of particles.

The elemental composition of all synthesized powders was determined using energy-dispersive spectroscopy, and the resulting data after processing the spectra are presented in Table 1, accounting for the carbon content of the conductive adhesive tape used during the sample preparation for analysis. It is noteworthy that all samples align with the experimentally derived chemical composition, with values falling within the error margin of the determination method (±0.5 at. %).

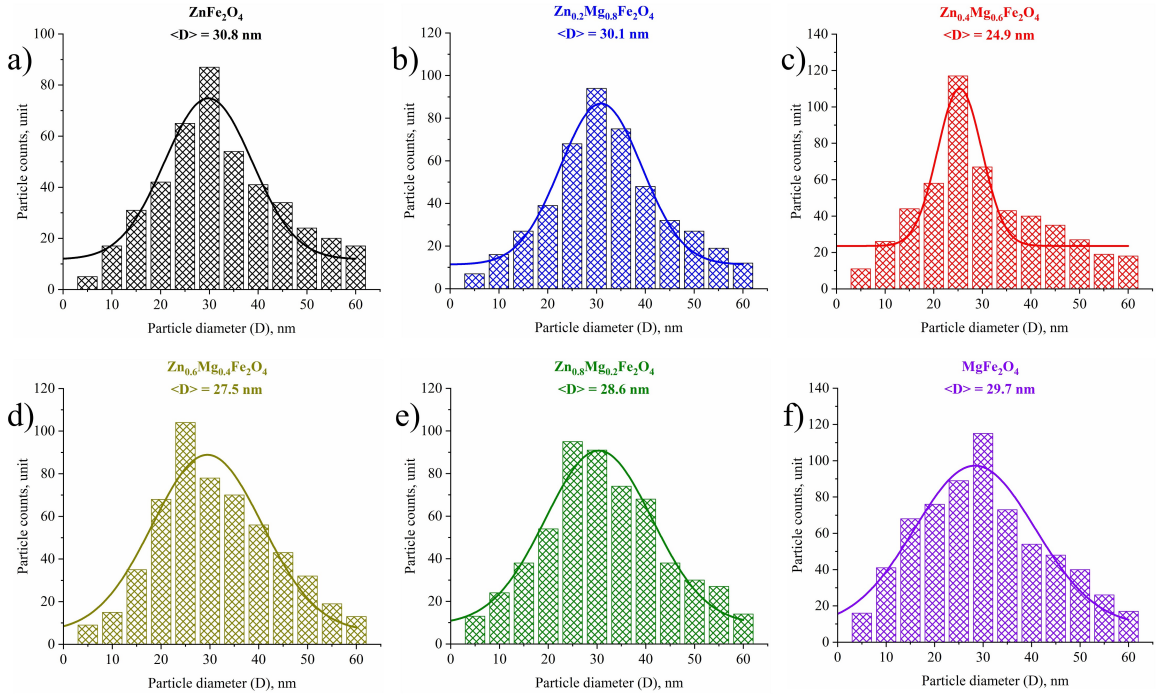

FIG. 2. Particle size distributions of $Zn_xMg_{1-x}Fe_2O_4$ (x = 0, 0.2, ..., 1.0) prepared by solution combustion method

TABLE 1. Elemental composition of synthesized zinc-magnesium ferrite samples

Sample	Zn, at. %	Mg, at. %	Fe, at. %
$ZnFe_2O_4$	32.7	0	67.3
$Zn_{0.8}Mg_{0.2}Fe_2O_4$	26.1	6.9	67.0
$Zn_{0.6}Mg_{0.4}Fe_2O_4$	18.6	11.8	69.6
$Zn_{0.4}Mg_{0.6}Fe_2O_4$	11.9	18.4	69.7
$Zn_{0.2}Mg_{0.8}Fe_2O_4$	7.1	25.8	67.1
$MgFe_2O_4$	0	33.1	66.9

Diffraction patterns of $Zn_xMg_{1-x}Fe_2O_4$-type ferrites (x = 0, 0.2, ..., 1.0) are depicted in Fig. 3a. It is evident that all synthesized samples exhibit a predominant phase, which, as per the ICDD PDF-2 database, corresponds to zinc-magnesium ferrite (JCPDS # 73-2211). The diffraction peaks across all samples exhibit similar width and intensity, with no discernible peaks of impurity phases, such as iron, zinc, and magnesium oxides. The average crystallite size was determined using the Scherrer formula and aligns well with the data presented in Fig. 2. Notably, the smallest crystallite size was calculated for the $Zn_{0.6}Mg_{0.4}Fe_2O_4$ sample, measuring 21.3 nm, slightly less than the visual estimate by SEM. This disparity is attributed to the difference between the actual particle size and the size of its crystalline core. Additionally, crystallite size distributions, as depicted in Figure 3b, were generated using the fundamental parameters method. These data also corroborate well with the results of visual assessment by SEM and calculations using the Scherrer formula. The distributions indicate that the average size across all samples falls within the range of 38 to 22 nm. Thus, the reproducibility of the results regarding average size determination was confirmed, validating the successful synthesis of $Zn_xMg_{1-x}Fe_2O_4$ system nanoparticles (x = 0, 0.2, ..., 1.0).

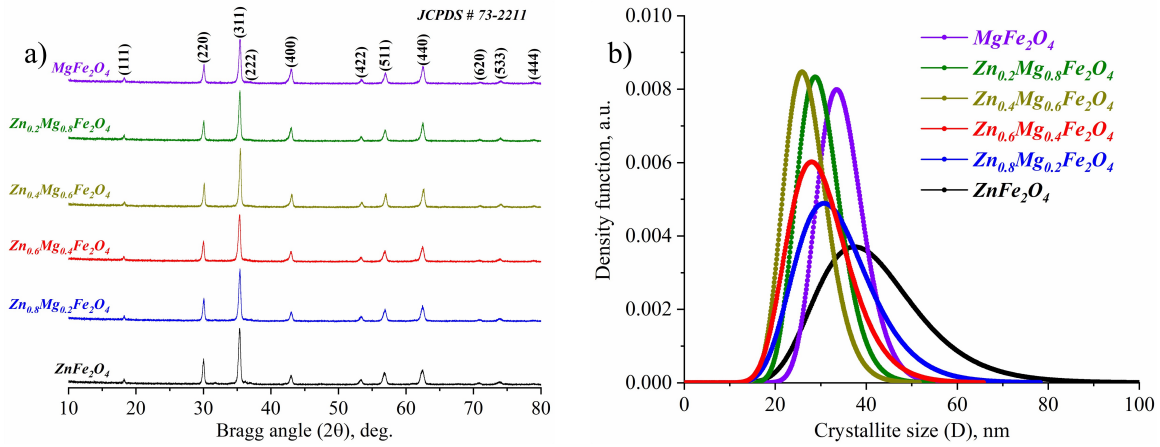

FIG. 3. Diffraction patterns of zinc-magnesium ferrite nanopowders with different amounts of magnesium

Using the Rietveld method, X-ray diffraction analysis was conducted for all synthesized compositions, enabling the determination of unit cell parameters and lattice volume. The provided values indicate minimal lattice stress across all samples, with stress levels below 0.5%. Of particular interest is the examination of changes in lattice parameters, as the substitution of Mg^{2+} cations with Zn^{2+} exerts a significant influence on these characteristics. Indeed, structural parameters play a pivotal role in dictating the magnetic and electrochemical behavior of spinel ferrites. Calculation was performed utilizing the main crystallographic directions (220), (311), (400), and (440), characterized by their high intensity and excellent agreement with standard peaks. The lattice parameter (a = b = c) for pure magnesium ferrite was determined to be 8.416 Å, consistent with reference card data (JCPDS # 73-2211), and decreases progressively with an increasing proportion of Mg^{2+} cations. This trend is attributed to the disparity in ionic radii between Zn^{2+} (0.82 Å) and Mg^{2+} (0.65 Å), a finding supported by existing literature [21]. However, it's worth noting that the potential for the substitution of Fe^{3+} cations at tetrahedral positions may induce slight variations in lattice parameter growth rates. This phenomenon may explain the modest decrease observed in lattice parameters for the $Zn_{0.8}Mg_{0.2}Fe_2O_4$ and $Zn_{0.6}Mg_{0.4}Fe_2O_4$ samples. Furthermore, the obtained dependencies align well with changes in average crystallite size, thereby indirectly validating structural alterations.

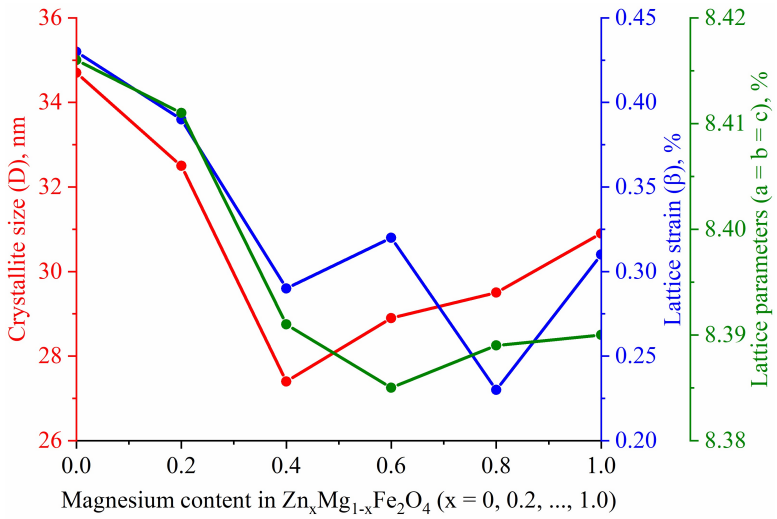

FIG. 4. Average crystallite size, lattice stress and lattice parameters of zinc-manganese ferrite nanopowders

Magnetic M-H hysteresis loops, recorded at room temperature using a standard cell, are illustrated in Fig. 4a. The appearance of these hysteresis loops distinctly showcases the influence of magnesium cation doping on the magnetic behavior of zinc-magnesium ferrites, particularly concerning saturation and coercive force.

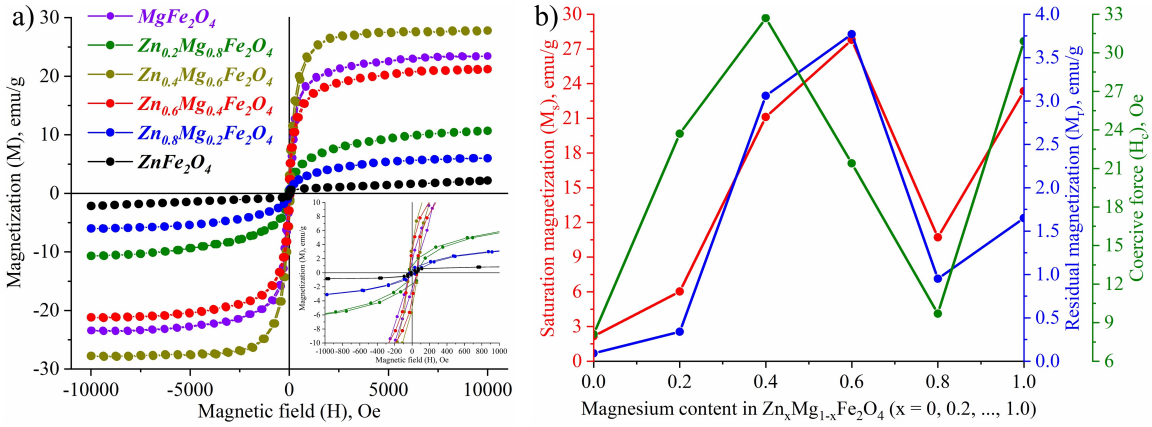

FIG. 5. M-H hysteresis loops of $Zn_{0.6}Mg_{0.4}Fe_2O_4$ synthesized by solution combustion method

To facilitate analysis of the primary magnetic parameters obtained (saturation magnetization, saturation remanent magnetization, and coercive force), their dependencies on the number of magnesium cations (x) in the sample compositions were plotted (Fig. 5b). These graphs reveal that pure zinc ferrite exhibits the lowest magnetic parameters (Ms = 2.16 emu/g, Mr = 0.09 emu/g, and Hc = 8.1 Oe). Moreover, a significant enhancement in magnetic characteristics is observed with increasing magnesium proportion in the spinel crystal lattice, peaking at x = 0.4 ($Zn_{0.4}Mg_{0.6}Fe_2O_4$ sample) with values of 27.78 emu/g, 3.77 emu/g, and 32.7 Oe, respectively. Subsequently, due to ongoing structural alterations and the substitution of Mg^{2+} cations with Zn^{2+} and Fe^{3+} cations at tetrahedral positions, magnetic characteristics begin to decline, continuing through to the $Zn_{0.2}Mg_{0.8}Fe_2O_4$ sample. Ferrite fully substituted by magnesium cations exhibits magnetic parameters characteristic of pure $MgFe_2O_4$, aligning well with literature data [24].

Fig. 6 displays cyclic voltammograms of synthesized nanoparticles of multicomponent zinc-magnesium ferrites. Measurements were conducted in a 1 M KOH alkaline electrolyte at a constant scanning speed of 10 mV/s within a potential window of -2 – 2.0 V, ranging from -1800 to 1600 mV relative to the silver chloride electrode. Notably, all samples, except for pure zinc ferrite, exhibit nearly identical coverage areas. The most pronounced cathodic peak is observed in the $ZnFe_2O_4$ sample at 0.58 V, while the anodic peak is recorded at 0.24 V. The appearance and retention of charge are attributed to redox reactions of the Fe^{3+}/Fe^{2+} type at the electrode. Consequently, the obtained capacity indicators primarily depend on the characteristics of these redox reactions, which are less pronounced in multicomponent zinc-magnesium and pure magnesium ferrite compared to zinc ferrite. The data suggests that all synthesized samples are theoretically suitable as starting materials for the production of electrochemical sensors.

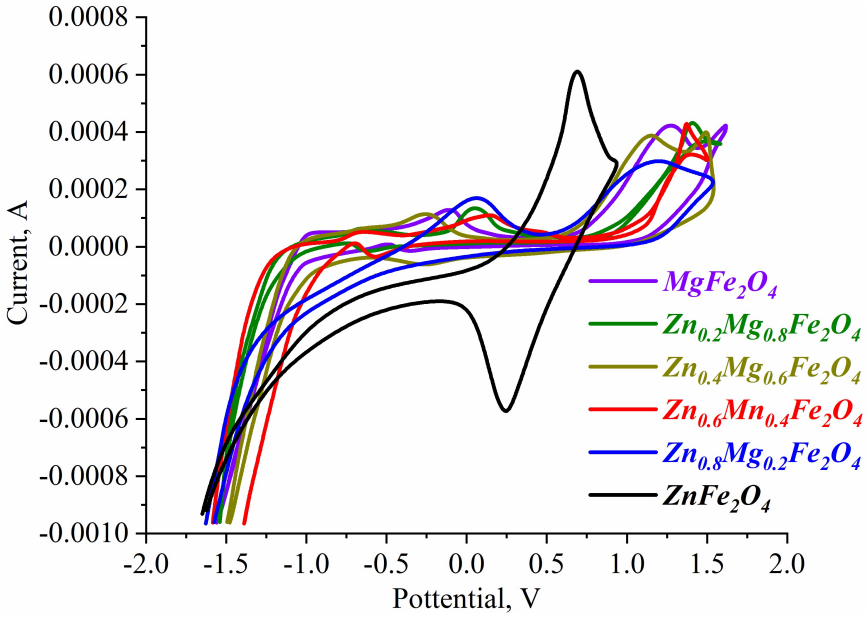

FIG. 6. M-H hysteresis loops of $Zn_{0.6}Mg_{0.4}Fe_2O_4$ synthesized by solution combustion method

4. Conclusion

In summary, this study focuses on the synthesis and characterization of multicomponent zinc-magnesium ferrites ($Zn_xMg_{1-x}Fe_2O_4$ type, with x ranging from 0 to 1.0) via solution combustion method utilizing glycine at a stoichiometric redox ratio. The average particle size of the synthesized samples ranged from 25 to 31 nm, with the amorphous phase constituting less than 5% of the composition. Phase analysis confirmed the absence of impurity oxide phases within the compositions. Structural parameter analysis revealed variations in unit cell parameters depending on the magnesium cation content, consequently influencing the primary magnetic characteristics in a nonlinear fashion, influenced by both particle size and structural alterations. Notably, samples with higher zinc content exhibited significant changes in hysteresis loop morphology. Analysis of cyclic voltammograms provided insights into the potential utilization of the synthesized powders as electrochemical materials.

References

[1] Varshney D., Verma K., Kumar A. Structural and vibrational properties of $Zn_xMn_{1-x}Fe_2O_4$ (x = 0.0, 0.25, 0.50, 0.75, 1.0) mixed ferrites. *Materials Chemistry and Physics*, 2011, **131**, P. 413–419.

[2] Martinson K.D., Ivanov A.A., Panteleev I.B., Popkov V.I., Effect of sintering temperature on the synthesis of LiZnMnFe microwave ceramics with controllable electro/magnetic properties. *Ceramics International*, 2021, **47**(21), P. 30071–30081.

[3] Dippong T., Levei E.A., Cadar O. Recent Advances in Synthesis and Applications of MFe_2O_4 (M = Co, Cu, Mn, Ni, Zn) nanoparticles. *Nanomaterials*, 2021, **11**, P. 1560.

[4] Salih S.J., Mahmood W.M. Review on magnetic spinel ferrite (MFe_2O_4) nanoparticles: From synthesis to application. *Heliyon*, 2023, **9**(6), P. e16601.

[5] Sahoo P., Choudhary P., Laha S.S., Dixit A., Mefford O.T. Recent advances in zinc ferrite ($ZnFe_2O_4$) based nanostructures for magnetic hyperthermia applications. *Chemical Communications*, 2023, **81**(59), P. 12065–12090.

[6] Sagayaraj R. A review on structural and magnetic properties of magnesium ferrite nanoparticles. *International Nano Letters*, 2022, **12**, P. 345–350.

[7] Nigam A., Saini S., Singh B., Rai A.K., Pawar S.J. Zinc doped magnesium ferrite nanoparticles for evaluation of biological properties viz antimicrobial, biocompatibility, and in vitro cytotoxicity. Materials Today: Communications, 2022, **31**, P. 103632.

[8] Wu K., Li J., Zhang C. Zinc ferrite based gas sensors: A review. *Ceramics International*, 2019, **45**(9), P. 11143–11157.

[9] Mahmoodi N.M. Zinc ferrite nanoparticle as a magnetic catalyst: Synthesis and dye degradation. *Materials Research Bulletin*, 2013, **48**(10), P. 4255–4260.

[10] Martinson K.D., Beliaeva A.D., Sakhno D.D., Beliaeva I.D., Belyak V.E., Nianikova G.G., Panteleev I.B., Naraev V.N., Popkov V.I. Synthesis, Structure, and Antimicrobial Performance of $Ni_xZn_{1-x}Fe_2O_4$ (x = 0, 0.3, 0.7, 1.0) Magnetic Powders toward E. coli, B. cereus, S. citreus, and C. tropicalis. *Water*, 2022, **14**(3), P. 454.

[11] Haghniaz R., Rabbani A., Vajhadin F., Khan T., Kousar R., Khan A.R., Montazerian H., Iqbal J., Libanori A., Kim H.-J., Wahid F. Anti-bacterial and wound healing-promoting effects of zinc ferrite nanoparticles. *Journal of Nanobiotechnology*, 2021, **19**, P. 38.

[12] Major J.L., Parigi G., Luchinat C., Meade T.J. The synthesis and in vitro testing of a zinc-activated MRI contrast agent. *PNAS*, 2007, **104**(35), P. 13881–13886.

[13] Rahman M.A., Islam M.T., Singh M.S.J., Samsuzzaman M., Chowdhury M.E.H. Synthesis and characterization of Mg–Zn ferrite based flexible microwave composites and its application as SNG metamaterial. *Scientific Reports*, 2021, **11**, P. 7654.

[14] Mishra B., Munisha B., Nanda J., Sankaran K.J., Suman S. Hydrothermally Synthesized Magnesium doped Zinc Ferrite Nanoparticles: An extensive study on structural, optical, magnetic, and dielectric properties. *Materials Chemistry and Physics*, 2022, **292**, P. 126791.

[15] Choudhury H.A., Choudhary A., Sivakumar M., Moholkar V.S., Mechanistic investigation of the sonochemical synthesis of zinc ferrite. *Ultrasonics Sonochemistry*, 2013, **20**(1), P. 294–302.

[16] Martinson K.D., Cherepkova I.A., Sokolov V.V. Formation of cobalt ferrite nanoparticles during the burning of glycine-nitrate and their magnetic properties. *Glass Physics and Chemistry*, 2018, **44**(1), P. 21–25.

[17] Bid S., Pradhan S.K. Preparation of Zinc Ferrite by High-Energy Ball-Milling and Microstructure Characterization by Rietveld's Analysis. *Materials Chemistry and Physics*, 2003, **82**(1), P. 27–37.

[18] Iqbal F., Mutalib M.I.A., Shaharun M.S., Khan M., Abdullah B. Synthesis of $ZnFe_2O_4$ Using sol-gel Method: Effect of Different Calcination Parameters. *Procedia Engineering*, 2016, **148**, P. 787–794.

[19] Riyanti F., Purwaningrum, W., Yuliasari N., Putri S., Apriani, N., Hariani P.L. The effect of fuel on the physiochemical properties of $ZnFe_2O_4$ synthesized by solution combustion method. *Turkish Journal of Chemistry*, 2022, **46**(6), P. 1875–1882.

[20] Senthamilselvan T., Nithiyanantham S., Kogulakrishnan K., Mahalakshmi S., Lakshmigandhan T., Mohan R., Gunasekaran B, Structural, magnetic, electric and electrochemical studies on zinc doped magnesium ferrite nano particles – Sol-gel method. *Heliyon*, 2024, **10**(3), P. E25511.

[21] Manikandan A., Vijaya J.J., Sundararajan M., Meganathan C., Kennedy L.J., Bououdina M. Optical and magnetic properties of Mg-doped $ZnFe_2O_4$ nanoparticles prepared by rapid microwave combustion method. *Superlattices and Microstructures*, 2013, **64**, P. 118–131.

[22] Heidari P., Masoudpanah S.M. Structural and magnetic properties of $MgFe_2O_4$ powders synthesized by solution combustion method: the effect of fuel type. *Journal of Materials Research and Technology*, 2020, **9**(3), P. 4469–475.

[23] Dyachenko S.V., Martinson K.D., Cherepkova I.A., Zhernovoi A.I. Particle size, morphology, and properties of transition metal ferrospinels of the MFe_2O_4 (M = Co, Ni, Zn) type, produced by glycine-nitrate combustion. *Russian Journal of Applied Chemistry*, 2016, **89**(4), P. 535–539.

[24] Dalt S.D., Takimi A.S., Volkmer T.M., Sousa V.C., Bergmann C.P. Magnetic and Mössbauer behavior of the nanostructured $MgFe_2O_4$ spinel obtained at low temperature. *Powder Technology*, 2011, **210**(2), P. 103–108.

Submitted 7 February 2024; accepted 15 March 2024

Information about the authors:

Kirill D. Martinson – Ioffe Institute, Politekhnicheskaya st., 26, St. Petersburg, 194064, Russia; ORCID 0000-0001-9313-4267; martinsonkirill@mail.ru

Alexander A. Murashkin – St. Petersburg Electrotechnical University "LETI", Professora Popova st., 5, St. Petersburg, 197022, Russia; murashkin1999@list.ru

Artem A. Lobinsky – Ioffe Institute, Politekhnicheskaya st., 26, St. Petersburg, 194064, Russia; lobinski.a@mail.ru

Danil D. Maltsev – Ioffe Institute, Politekhnicheskaya st., 26, St. Petersburg, 194064, Russia; ORCID 0000-0001-5787-0400; dm.work.ac@gmail.com

Kezhen Qi – College of Pharmacy, Dali University, Dali 671000, China; qkzh2003@aliyun.com

Jiaguo Yu – China University of Geosciences, 68 Jincheng St, Wuhan, 430078 P. R. China; yujiaguo93@cug.edu.cn

Oksana V. Almjasheva – St. Petersburg Electrotechnical University "LETI", Professora Popova st., 5, St. Petersburg, 197022, Russia; almjasheva@mail.ru

Vadim I. Popkov – Ioffe Institute, Politekhnicheskaya st., 26, St. Petersburg, 194064, Russia; vip-07@yandex.ru

Conflict of interest: the authors declare no conflict of interest.